Inorganic Chemistry

Article

pubs.acs.org/IC

Electronic Structure and Ligand Vibrations in FeNO, CoNO, and FeOO Porphyrin Adducts

Alexandra V. Soldatova, Mohammed Ibrahim,[†] and Thomas G. Spiro*

Department of Chemistry, University of Washington, Box 351700, Seattle, Washington 98195, United States

Supporting Information

ABSTRACT: The gaseous ligands, CO, NO, and O_2 interact with the Fe ion in heme proteins largely via backbonding of Fe electrons to the π^* orbitals of the XO (X = C, N, O) ligands. In these FeXO adducts, the Fe−X stretching frequency varies inversely with the X−O stretching frequency, since increased backbonding strengthens the Fe−X bond while weakening the X−O bond. Inverse frequency correlations have been observed for all three ligands, despite differing electronic and geometric structures, and despite variable composition of the "FeX" vibrational mode, in which Fe−X stretching and Fe−X−O coordinates are mixed for bent FeXO adducts. We report experimental data for 5-coordinate $Co^{II}(NO)$ porphyrin adducts (isoelectronic with $Fe^{II}(OO)$ adducts), and the results of density functional theory (DFT) modeling for 5-coordinate $Fe^{II}(NO)$, $Co^{II}(NO)$, and $Fe^{II}(OO)$ adducts. Inverse $\nu(MX)/\nu(XO)$ correlations are obtained computationally, using model porphyrins with graded electron-donating and -withdrawing substituents to modulate the backbonding. Computed slopes agree satisfactorily with experiment, provided nonhybrid functionals are used, which avoid overemphasizing high-spin states. The BP86 functional gives correct ground states, a closed-shell singlet for $Co^{II}(NO)$ and an open-shell singlet for the isoelectronic $Fe^{II}(OO)$, as corroborated by structural data for $Co^{II}(NO)$, and the $\nu(MX)/\nu(XO)$ slope agreement with experiment for both adducts. However, for $Fe^{II}(OO)$ adducts, the computed inverse $\nu(MX)/\nu(XO)$ correlation applies only to porphyrins with electron-donating and withdrawing substituents of moderate strength. For substituents more donating than $-CH_3$, a direct correlation is obtained, the Fe−O and O−O bonds weakening in concert. This effect is ascribed to the dominance of σ bonding via the in-plane $d_{xz}(+d_{z^2})$-π^* orbital, when electron-donating substituents raise the d orbital energies sufficiently to render backbonding (d_{yz}-π^*) unimportant.

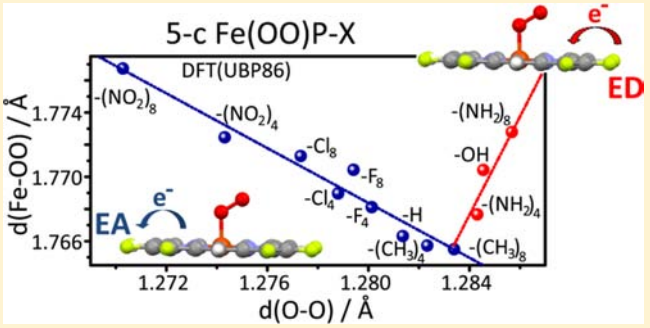

INTRODUCTION

The gaseous molecules CO, NO, and O_2, all constituents of the atmosphere, are also important signaling molecules in biology. The signaling receptor is generally a heme protein, to which the XO molecule binds, and initiates a conformation change that induces further biochemical events.[1−3] The heme prosthetic group is poised to bind these diatomic ligands, because they all have low-lying π^* orbitals, which can interact with d_π orbitals on the heme Fe. The resulting d_π-π^* backbonding is a key determinant of the binding affinity.

The binding event is also controlled by secondary interactions with the protein, involving a proximal ligand to the heme Fe, generally a histidine or cysteine side chain, and a variety of steric and electronic interactions with side chains that are distal to the heme-bound XO molecule. These interactions are also responsible for transducing the XO binding into protein conformation change.

Vibrational spectroscopy provides a useful probe of heme-XO binding, since the Fe−X and X−O stretching frequencies reflect the bond strengths, as modulated by the protein.[4−6] In general, these frequencies correlate inversely, because backbonding strengthens the Fe−X bond while weakening the X−O bond.[7,8] Electrostatic effects that increase or decrease backbonding can be gauged from these correlations. Other interactions that alter the geometric or electronic structure can be evaluated by the resulting deviations from the inverse correlations.[7−10]

Systematics for these effects have been worked out most thoroughly for FeCO porphyrin adducts,[8,9,11] which have the simplest FeXO electronic structure. CO has empty π^* orbitals and the $Fe^{II}(CO)$ adduct is linear, with backbonding interactions in both perpendicular directions. Computational modeling has been important for understanding the experimental data. Density functional theory (DFT) calculations on FeCO adducts of model porphyrins have reproduced the observed backbonding trends satisfactorily, and have illuminated the sources of deviations in secondary interactions.[9,12,13]

Studies have also been extended to NO, which has an extra electron, resulting in bent $Fe^{II}(NO)$ adducts.[8,13,14] The extra π^* electron is involved in σ bonding, but backbonding remains available perpendicular to the bending plane (Supporting

Received: February 12, 2013
Published: June 13, 2013

   dx.doi.org/10.1021/ic400364x | Inorg. Chem. 2013, 52, 7478−7486

Information, Figure S1). Also encountered, however, are $Fe^{III}(NO)$ complexes, which are isoelectronic with $Fe^{II}(CO)$, but have altered polarity, and quite different secondary interactions.[15−18] The important $Fe^{II}(OO)$ adducts are less-well studied, primarily because of experimental difficulties,[19−21] but useful data are accumulating.[22−36] O_2 has two π^* electrons, and the complex FeOO electronic structure has been much investigated recently.[37−45] The aim of the present work is to understand trends in the FeOO vibrational frequencies, extending the computational approach developed for FeCO and FeNO adducts. We have included $Co^{II}(NO)$ adducts in the study, and provide new experimental data on these adducts. $Co^{II}(NO)$ is isoelectronic with $Fe^{II}(OO)$, but has properties closer to $Fe^{II}(NO)$; it represents an intermediate case.

The present work is limited to 5-coordinate adducts. The effects of axial ligation and of other secondary interactions will be considered in a subsequent study.

MATERIALS AND METHODS

Resonance Raman Measurements. To obtain vibrational frequencies for 5-coordinate $Co^{II}(NO)$ adducts, four cobalt(II) porphyrin complexes were obtained from Porphyrin Systems, (Germany): meso-Tetraphenylporphyrin (Co(II)TPP); 5,10,15,20-Tetrakis-(4-methoxyphenyl)-porphyrin (Co(II)TMeOPP); 5,10,15,20-Tetrakis(2,6-difluorophenyl)porphyrin ($Co(II)TF_2PP$); 5,10,15,20-Tetrakis-(2,3,4,5,6-pentafluorophenyl)-porphyrin ($Co(II)TF_5PP$), and 5,10,15,20-Tetrakis-(mesityl)-porphyrin (Co(II)TMP) was obtained from Midcentury Chemicals (Posen, IL). Co(II) porphyrin solutions in CH_2Cl_2 (~5 mM) were prepared by transferring, under Ar gas, deoxygenated CH_2Cl_2 into sealed, deoxygenated vials containing the Co(II) porphyrin samples. Portions of the solution were transferred, under Ar gas, to a sealed, previously deoxygenated NMR tube. ^{14}NO gas, chemically generated by reduction of sodium nitrite with ascorbate, was added, via a gastight syringe, to the Co(II) porphyrin solution in the NMR tube to form $Co^{II}(^{14}NO)P$ adduct. Samples of $Co^{II}(^{15}NO)P$ were prepared in a similar way using ^{15}NO gas.

Resonance Raman (RR) spectra were obtained via backscattering geometry at room temperature in spinning NMR tubes. The excitation wavelengths of 406.7 and 413 nm were obtained by frequency doubling, via a lithium triborate crystal, a Ti:sapphire laser (Photonics International TU-UV), which was pumped by the second harmonic of a Q-switched Nd:YLF laser (Photonics Industries International, GM-30-527). These laser wavelengths were confirmed with an Ocean Optics UV−vis spectrometer (Model USB2000+). The laser power at the sample was kept to a minimum (<1 mW) by using a cylindrical lens, to minimize the photodissociation of the NO adducts. Scattered light was collected and focused onto a triple spectrograph (Spex 1877) equipped with a CCD detector (Roper Scientific, Model 7375-0001) operating at −110 °C. Each spectrum was averaged over 15 min of acquisition. Spectra were calibrated with dimethylsulfoxide-d_6 and analyzed with Grams A/I (Thermo-Galactic).

DFT Calculations. Density functional theory (DFT) calculations on 5-coordinate model complexes were performed using the Gaussian 03 or 09 programs.[46,47] The standard 6-31G* basis set was used for all the atoms except Fe and Co, which were described by the Ahlrichs' valence triple-ζ (VTZ) basis set.[48] Geometry optimization and frequency calculations were performed using tight convergence criteria and an ultrafine integration grid. C_s symmetry was assumed for the model porphyrins with eight substituents, except for $-NO_2$ substituents. For the latter, C_s symmetry constraint resulted in small imaginary frequencies corresponding to $-NO_2$ group rotations; a stable C_1 structure was found instead. The models having four porphyrin substituents and protoporphyrin models were optimized without symmetry constraints. Vibrational frequency values for the optimized structures were taken directly from the Gaussian program without scaling. $Fe^{II}(NO)$ models were optimized with the unrestricted BP86 (UBP86) functional, assuming a doublet ground state. $Co^{II}(NO)$ and $Fe^{II}(OO)$ models were first optimized with the BP86 functional assuming a closed shell singlet ground state. The closed shell wave function was then tested for the presence of spin unrestricted, lower energy solutions using the STABLE = OPT key in Gaussian. When the RHF→UHF instability was found and an open shell singlet wave function was located, the geometry was reoptimized using the newly found open shell singlet wave function. In the case of the $Co^{II}(NO)$ complexes, the closed singlet ground state was the lowest energy configuration with the BP86 functional. In the case of the 5-c $Fe^{II}(OO)$ models, an open shell singlet state was the lowest electronic configuration. For the unsubstituted $Fe^{II}(OO)P$ complex in the open shell singlet, Gaussian 09 experienced a problem with SCF convergence; thus, the results for this complex were obtained with the Gaussian 03 version, which apparently did not have the same issue. Other functions, both pure and hybrid, were also tested during geometry optimization of the simple porphine complex of each model. The results are given in Supporting Information, Tables S1−S3. The choice of BP86 functional to calculate vibrational stretching frequencies correlation is justified in the Results section.

RESULTS

Mode Assignments. The assignment of metal−ligand vibrational modes in bent FeXO adducts is complicated by the fact that mixing of stretching and bending coordinates is permitted by symmetry. The inherent frequency is similar for Fe−X stretching and Fe−X−O bending, and mixing of these two coordinates is therefore substantial. (XO stretching is much higher in frequency, so that mixing with other coordinates is inconsequential.) The result is that two normal modes in the 400−600 cm^{-1} region have major contributions from Fe−X stretching and Fe−X−O bending coordinates. The percentage contributions vary from case to case. The resulting assignment ambiguity has been discussed extensively.[13,49−51]

The Fe−X stretching and Fe−X−O bending coordinates have the same phase in the lower frequency mode and the opposite phase in the higher frequency mode. Experimentally, the higher frequency mode experiences a larger frequency shift upon isotopic substitution of the X atom. It also has higher intensity in RR spectra. Indeed the lower frequency mode is generally hard to detect.[51,52] We have found[13] that the higher frequency mode correlates with the X−O stretching mode in a manner similar to the correlation of ν(FeC) and ν(CO) in $Fe^{II}(CO)$ adducts, for which mixing with Fe−C−O bending is precluded by symmetry. For simplicity, we label this RR-detectable, isotope-sensitive mode "νFeX", recognizing that it necessarily contains some contribution, possibly a large one, from Fe−X−O bending.

$Co^{II}(NO)$ Spectra. Our laboratory has previously used RR spectroscopy to locate ν(CoN) and ν(NO) in several 5-c CoNO porphyrin adducts (Table 1) to establish that the NO adduct of Co-substituted sGC (soluble guanylate cyclase) also contains a 5-c $Co^{II}(NO)$ protoporphyrin.[53] In the present study, we examine backbonding effects on the Co−NO and N−O frequencies, by employing a series of tetraphenylporphyrin adducts with a variety of electron-donating or withdrawing substituents on the phenyl rings, a method applied previously to $Fe^{II}(CO)$ and $Fe^{II}(NO)$ porphyrin adducts.[13,22] Figure 1 shows RR and isotope difference spectra for the 5-c $Co^{II}(NO)$ adducts of porphyrins with electron donating (tetra-mesityl) and withdrawing (tetra-difluorophenyl) substituents. The RR spectra are dominated by the expected porphyrin modes,[5,54] but the ν(CoN) and ν(NO) modes are readily identified in the $^{14/15}NO$ difference spectra, as is the δ(Co−N−O) mode. Spectra for several other $Co^{II}(NO)$ porphyrins are displayed in

dx.doi.org/10.1021/ic400364x | Inorg. Chem. 2013, 52, 7478−7486

Table 1. Co^{II}–NO and N–O Stretching Frequencies (cm^{-1}) of Five-Coordinate Co^{II}(NO) Porphyrin Adducts

complex	ν(Co–NO) ($\Delta^{14}NO/^{15}NO$)	ν(N–O) ($\Delta^{14}NO/^{15}NO$)	solvent	reference
Co(II)(TPP)(NO)	514 (22)	1692 (30)	CH_2Cl_2	this work
Co(II)(TMP)(NO)	517 (16)	1680 (30)	CH_2Cl_2	this work
Co(II)(TPP-p-OMe)(NO)	519 (21)	1682 (30)	CH_2Cl_2	this work
Co(II)(TF_2PP)(NO)	513 (16)	1699 (30)	CH_2Cl_2	this work
Co(II)(TF_5PP)(NO)	501 (17)	1709 (32)	CH_2Cl_2	this work
Co(II)(OEP)(NO)	521 (17)	1673 (30)	CH_2Cl_2	53
Co(II)(PPIXDME)(NO)	519	1678	CH_2Cl_2	53
Co(II)MO sGC_1	523 (26)	1675 (37)	25 mM TEA buffer, pH 7.4	53

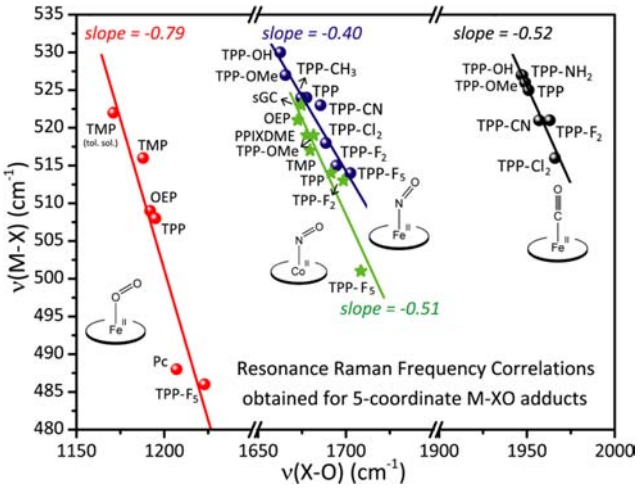

Figure 2. RR ν_{MX}/ν_{XO} correlation plots obtained for the five-coordinate Fe^{II}(XO) and Co^{II}(NO) porphyrin complexes. For the Fe^{II}(CO) adducts (black points): data from ref 55; for the Fe^{II}(NO) adducts (blue points): data from ref 22; for five-coordinate Fe^{II}(OO) (red points): data from refs 23–25, 56 (see Supporting Information, Table S4 for details); data points for five-coordinate Co^{II}(NO) (green stars) are obtained in this work (Table 1).

Supporting Information, Figures S2–S4, and the frequencies are collected in Table 1.

As expected from backdonation, the ν(NO) frequency systematically increases while ν(CoN) decreases when the substituents become increasingly electron-withdrawing. The newly obtained ν(CoN) and ν(NO) frequencies plotted together with available points from the literature give a linear negative correlation, just as do other 5-c M^{II}(XO) porphyrins (Figure 2).

When the Co^{II}(NO) backbonding correlation plot is compared to the correlation plots obtained experimentally for similar TPP substituents of the Fe^{II}(CO), Fe^{II}(NO), and Fe^{II}(O_2) series in Figure 2, it is apparent that for these four adducts, the backbonding correlations are quite similar, albeit with different slopes. The slope of the backbonding correlation lines reflects the sensitivity of the adducts to metal $d_\pi \rightarrow \pi^*_{XO}$ backbonding mechanism. The Fe^{II}(CO), Fe^{II}(NO), and Co^{II}(NO) adducts are similarly responsive to the backbonding modulation, while Fe^{II}(O_2) adducts, having the highest slope, are least responsive to backbonding.

DFT Modeling. Appropriate choice of the DFT functional is essential for proper modeling of heme-ligand interactions. We have successfully modeled the vibrational frequency backbonding trend for Fe^{II}(CO) porphyrin adducts using the popular hybrid functional, B3LYP.[13,22] Although the frequencies themselves are overestimated, as usual with DFT,[57] negative ν(FeC)/ν(CO) correlations were obtained for both 5- and 6-coordinate adducts, with slopes that were close to the experimentally determined ones. However, B3LYP was less successful for Fe^{II}(NO) adducts,[13] because of its tendency, common to hybrid functionals, to overestimate the stability of high-spin states.[58] Less spin contamination and more accurate bond distances were obtained with the pure functional, BLYP[13] (Supporting Information, Table S1).

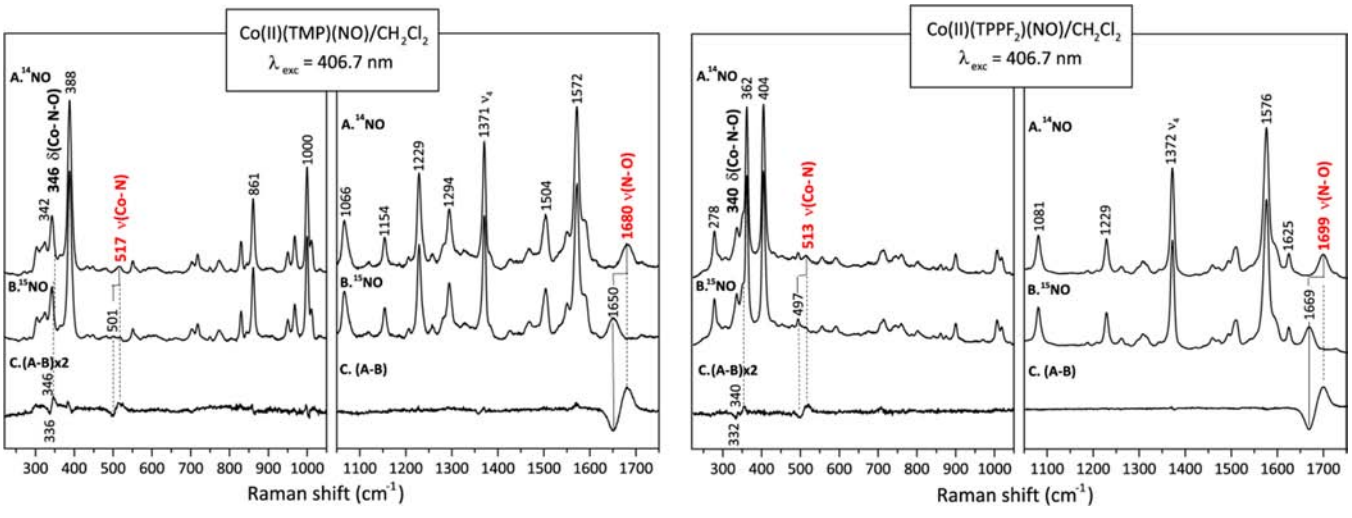

Figure 1. RR spectra and difference spectra ($^{14}NO-^{15}NO$) (low-frequency region, left; high frequency region, right) for Co(II)TMP(NO) and Co(II)($TPPF_2$)(NO), in CH_2Cl_2 solution.

dx.doi.org/10.1021/ic400364x | Inorg. Chem. 2013, 52, 7478–7486

The spin level problem is even more significant for $Co^{II}(NO)$ and $Fe^{II}(OO)$ adducts, for which open- and closed-shell singlet states are close in energy.[58,59] We explored a number of functionals (Supporting Information, Tables S2, S3) and found a closed-shell ground state for $Co^{II}(NO)$ with pure functionals, and bond distances that are in reasonable accord with experiment (Supporting Information, Table S2). However, the hybrid functionals gave a lower energy for the open-shell configuration, whose computed Co−NO bond distance is significantly longer than experimentally determined ones (Supporting Information, Table S2). Similar CoNO porphyrin results were reported for B3LYP vs. BP86 or BLYP functionals by Jaworska,[60,61] and studies of the related cobalamin molecule with alkyl or NO ligands likewise indicated superior performance for the nonhybrid functionals.[59,62] B3LYP was found to underestimate the ligand binding energies and overestimate the Co−N distance to the axial ligand.

Many DFT calculations have been reported for FeOO porphyrins.[37−41,44,63,64] There is general agreement that the ground state is an open-shell singlet.[39−44] (No experimental structures are available for 5-coordinate FeOO adducts, so the computed structural parameters (Supporting Information, Table S3) do not provide guidance.) Thus, although $Co^{II}(NO)$ and $Fe^{II}(OO)$ adducts are isoelectronic, they have different ground states.

The FeOO spin-density distribution, shown in Figure 3, reveals opposed but localized spins on the OO and Fe fragments in the open-shell singlet ground state. Shown for comparison is the spin-density distribution for $Fe^{II}(NO)$ adducts, which have a doublet ground state, the lone unpaired electron being distributed over the NO and Fe orbitals.

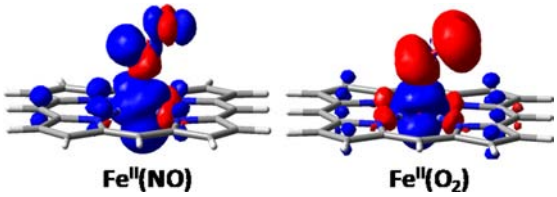

Figure 3. Spin density distribution in the $Fe^{II}(NO)$ and $Fe^{II}(O_2)$ models obtained from the DFT/UBP86 calculations. Spin-up and spin-down densities are shown as red and blue areas, respectively.

In view of its superior predictions of ground states and structures, we limit the subsequent discussion to computations with the BP86 functional (restricted BP86 for $Co^{II}(NO)$, and unrestricted BP86 for the $Fe^{II}(NO)$ and $Fe^{II}(O_2)$ adducts), although results with other functionals can be found in the Supporting Information. The computed structures for $Fe^{II}(NO)$, $Co^{II}(NO)$ and $Fe^{II}(OO)$ adducts of porphine are shown in Figure 4. In each case the optimization left the XO ligand oriented between adjacent pyrrole rings, presumably to minimize nonbonded repulsions.

Computed Vibrational Trends. As in previous studies,[13,15,22] we investigated changes in electron density at the central metal ion by attaching electron-donating or -withdrawing substituents to the porphyrine periphery (Figure 5). Structures and vibrational frequencies were computed to examine the ν(MX)/ν(XO) correlations.

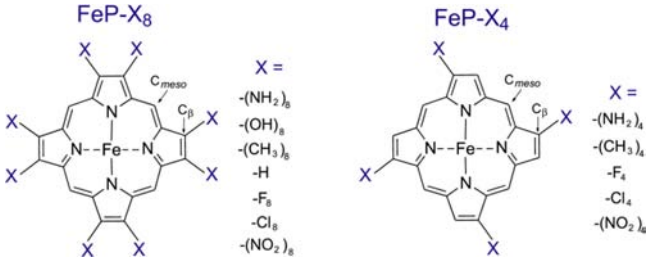

Figure 5. Structural diagram for FeP−X_8 and FeP−X_4 porphyrins used to model the backbonding trend. −X are indicated substituents, where −X_4 implies that −X and −H substituents alternate around the ring.

The substitutions were limited to the pyrrole C_β atoms, because direct substitutions at the methine bridges (C_{meso}) specifically influence the porphyrin a_{2u} molecular orbital, which in turn interacts with the d_{z^2} orbital of the central metal ion, altering its relative energy.[15] This interaction can have consequences beyond the general inductive effect of the C_β substituents, which we employ to modulate backbonding. The trends compare well with the experimental data, even though these involved changing the X atom on the phenyl−X ring, which is itself attached to the C_{meso} atoms. The phenyl ring attenuates electronic communication with −X, so that only the inductive effect is expressed.

The "ν(FeX)" mode was chosen as the calculated mode in the 400−600 cm^{-1} region having the largest Fe-X displacement.

$Fe^{II}(NO)$ adducts. We have previously reported computations for $Fe^{II}(NO)$ adducts using the UBLYP functional.[13] Satisfactory bond distances were obtained, and the computed ν(FeN) and ν(NO) frequencies correlated negatively for 6-coordinate adducts having imidazole axial ligands, with a slope similar to that observed experimentally. However, the results for 5-coordinate adducts were scattered.[13]

We have now re-examined the 5-coordinate correlation using the UBP86 functional and a larger set of porphyrin substituents (Table 2). A negative linear correlation ν(FeN)/ν(NO) was obtained (r = 0.96), with a slope of −0.26, in decent agreement with the experimental slope, −0.40 (Figure 6). The same set of substituted porphyrins calculated with the UBLYP functional gave more scattered frequencies data points resulting in a poorer ν(FeN)/ν(NO) correlation (slope = −0.19, r = 0.91)

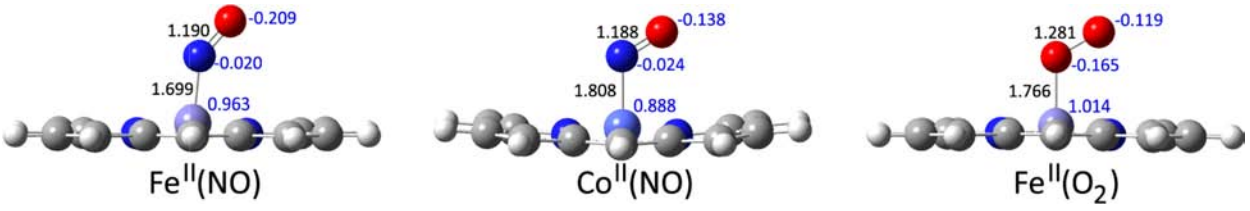

Figure 4. Optimized structures of 5-coordinate $Fe^{II}(NO)P$, $Co^{II}(NO)P$, and $Fe^{II}(OO)P$. Indicated are bond distances (Å, black) and Mulliken charges (blue).

dx.doi.org/10.1021/ic400364x | Inorg. Chem. 2013, 52, 7478−7486

Table 2. Optimized (DFT, UBP86) Bond Lengths (Å), Bond Angles (deg), and Vibrational Stretching Frequencies (cm^{-1}) Obtained for the Five-Coordinate $Fe^{II}(NO)$ Porphine Adducts with Different β-Substituents, Including Those of Protoporphyrin, $FePP(PropH)_2$

complex	Fe−NO	N−O	∠FeNO	$Fe-N_p$	ν(Fe−NO)	ν(N−O)
			5-c Fe(II)NO, UBP86 Functional			
$FeP(NH_2)_8$	1.696	1.194	143.6	2.005/2.036	622.4	1715
$FeP(CH_3)_8$	1.698	1.192	143.6	2.002/2.032	621.8	1721
$FePP(PropH)_2$	1.699	1.190	143.9	2.006/2.031	620.3	1727
FePH	1.699	1.190	143.9	2.002/2.031	621.3	1731
$FePF_4$	1.700	1.189	144.0	2.000/2.029	618.2	1736
$FePF_8$	1.701	1.188	143.8	1.998/2.027	616.1	1738
$FePCl_8$	1.702	1.186	144.2	2.006/2.035	616.8	1747
$FeP(NO_2)_4$	1.706	1.184	144.4	2.006/2.034	614.0	1755
$FeP(NO_2)_8$	1.710	1.180	144.6	2.003/2.031	607.2	1771

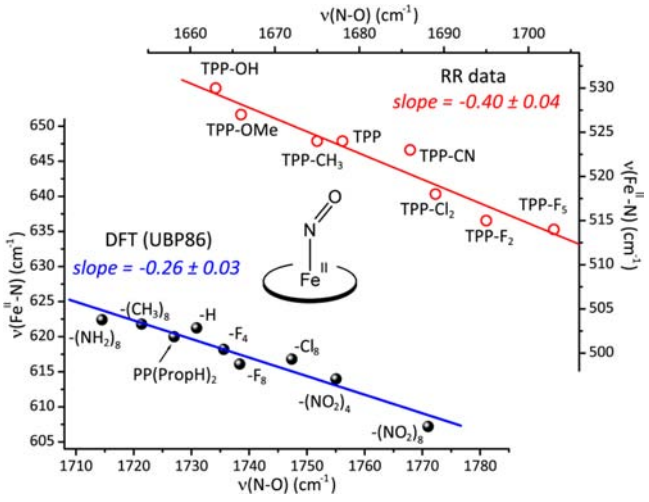

Figure 6. ν_{FeN}/ν_{NO} correlation computed for the five-coordinate $Fe^{II}(NO)PX_8$ and $Fe^{II}(NO)PX_4$ complexes (black points) and experimentally obtained (red points). $PP(PropH)_2$ point corresponds to $Fe^{II}(NO)$ protoporphyrin with protonated propionates. Linear correlations are shown for RR data (red line, r = 0.97), and for the theoretical models (blue line, r = 0.96).

(Supporting Information, Figure S5), though the bond length correlation d(Fe−NO)/d(N−O) was similar with the two functionals (Supporting Information, Figure S6).

$Co^{II}(NO)$ Adducts. In agreement with the available experimental structures (Supporting Information, Table S2), the $Co^{II}(NO)$ models are calculated to have a bent CoNO unit, with CoNO angle of ∼120°. As expected from backbonding, the Co−NO bond length decreases and the N−O bond increases when substituents become increasingly electron-donating (Table 3 and Supporting Information, Figure S7). The same methodology applied to CoNO adducts gives a set of ν(CoN)/ν(NO) points for a similar series of porphyrin substituents (Table 3), which again describes a negative linear correlation (Figure 7). The slope, −0.54, is slightly higher than that obtained experimentally for the CoTPP-X adducts, −0.51. Computed and experimental slopes are both higher for $Co^{II}(NO)$ than for $Fe^{II}(NO)$ adducts.

$Fe^{II}(OO)$ Adducts. The same methodology applied to $Fe^{II}(OO)$ adducts (Table 4) gives a more complex result (Figure 8). For substituents more electron-withdrawing than $-CH_3$, a negative ν(FeO)/ν(OO) correlation is obtained, with a slope, −0.64, close to that given by the available experimental data, −0.79. However, the correlation levels out for the strongly electron-withdrawing $-Cl_8$ and $-NO_2$ substituents, for which the computed ν(Fe−O) stays above 500 cm^{-1}. This leveling effect is not seen, however, if computed distances, rather than frequencies are correlated. Figure 9 shows a linear variation of d(Fe−O) with d(O−O) for all electron withdrawing substituents. The leveling effect in the frequency correlation represents a breakdown in correlation of bond distance and vibrational mode frequency, possibly reflecting a shift in the computed mode composition.

More striking is the slope reversal, in both ν(FeO)/ν(OO) and d(Fe−O)/d(O−O) plots, for porphyrin substituents more electron-donating than $-CH_3$. In this region of both plots, a strongly positive correlation is seen.

Table 3. Optimized (DFT, BP86) Bond Lengths (Å), Bond Angles (deg), and Vibrational Stretching Frequencies (cm^{-1}) Obtained for the Five-Coordinate $Co^{II}(NO)$ Porphine Adducts with Different β-Substituents

complex	Co−NO	N−O	∠CoNO	$Co-N_p$	ν(Co−NO)	ν(N−O)
			5-c Co(II)NO, BP86 Functional			
$CoP(NH_2)_8$	1.799	1.191	121.2	1.986/2.010	594	1688
$CoP(CH_3)_8$	1.805	1.190	121.1	1.980/2.003	590	1695
$CoPP(PropH)_2$	1.806	1.189	121.1	1.982/2.001	588	1700
CoPH	1.808	1.188	121.1	1.979/2.002	588	1704
$CoPF_4$	1.809	1.187	121.1	1.981/2.004	584	1710
$CoPF_8$	1.810	1.186	121.0	1.979/2.002	582	1714
$CoPCl_8$	1.813	1.184	121.1	1.983/2.005	579[a]	1720
$CoP(NO_2)_4$	1.822	1.182	121.1	1.972/1.994	576[a]	1729
$CoP(NO_2)_8$	1.829	1.179	121.1	1.968/1.989	561[a]	1746

[a]Averaged values over several modes with significant Co−NO displacement.

dx.doi.org/10.1021/ic400364x | Inorg. Chem. 2013, 52, 7478−7486

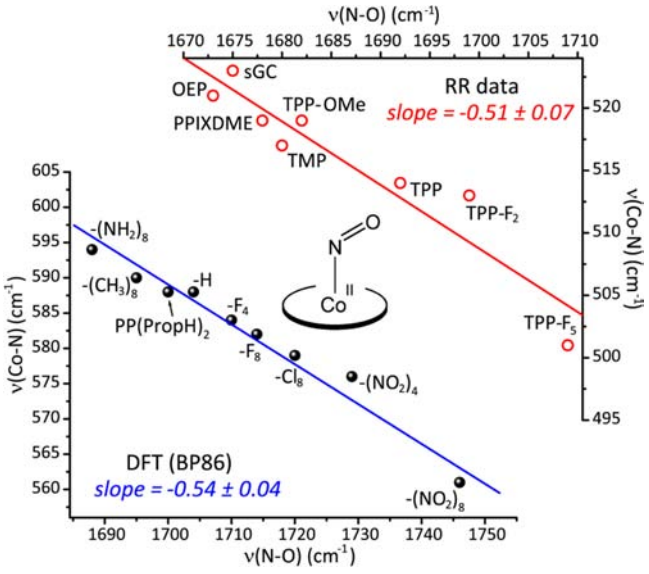

Figure 7. ν_{CoN}/ν_{NO} correlation plots computed for the five-coordinate $Co^{II}(NO)PX_8$ complexes (black points) and experimentally obtained (red points). $PP(PropH)_2$ point corresponds to $Co^{II}(NO)$ protoporphyrin with protonated propionates. Linear correlations are shown for RR data (red line, r = 0.94), and for the theoretical models (blue line, r = 0.98).

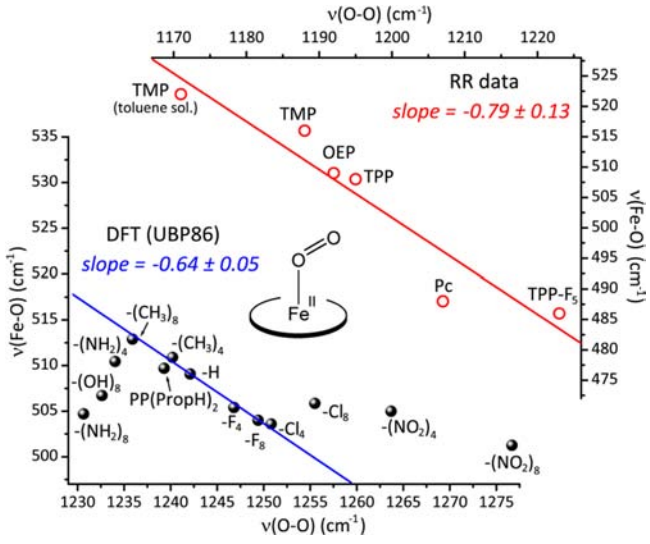

Figure 8. ν_{FeO}/ν_{OO} correlation plots computed for the five-coordinate $Fe^{II}(OO)PX_8$ and $Fe^{II}(OO)PX_4$ complexes (black points) and experimentally obtained for selected matrix-isolated $Fe^{II}(O_2)$ porphyrins (red points). Linear correlations are shown for RR data (red line, r = 0.95), and for the theoretical models (blue line, r = 0.99), but excluding the $-Cl_8$, $-(NO_2)_4$, $-(NO_2)_8$, $-(NH_2)_8$, $-(OH)_8$, $-(NH_2)_4$ data points.

We also computed BP86 frequencies and bond distances for the same set of $Fe^{II}(OO)$ adducts in the closed shell singlet state, which is slightly higher in energy than the open shell singlet ground state (Supporting Information, Table S6). The results, shown in Supporting Information, Figure S8, are qualitatively similar but the slope of the negative part of the $\nu(FeO)/\nu(OO)$ correlation, −0.24, is much lower than that obtained in the ground state, or seen in the experimental data.

DISCUSSION

The similar negative $\nu(FeX)/\nu(XO)$ correlations seen for all three XO molecules, CO, NO, and OO, demonstrate the overriding importance of backbonding in all these adducts, despite differences in electronic and geometric structure. $Fe^{II}(CO)$ is linear, while $Fe^{II}(NO)$ and $Fe^{II}(OO)$ are increasingly bent, with one and two additional electrons in the XO π^* orbitals, respectively. Linear $Fe^{II}(CO)$ has two backbonding interactions, the two CO π^* orbitals overlapping with the Fe d_{xz} and d_{yz} orbitals, while the bent $Fe^{II}(NO)$ and $Fe^{II}(OO)$ adducts have only one backbonding interaction, perpendicular to the FeXO bending plane of FeNO and FeOO. However, the π^* orbital energies are lower for NO and OO than for CO, and interact more effectively with the Fe orbitals. The present results show that $Co^{II}(NO)$ adducts likewise fall into this pattern.

Moreover, the correlations are similar despite the fact that the compositions of the "ν(MX)" modes differ. They are purely M−X stretching for linear FeCO, but mixed M−X stretching and M−X−O bending for the bent MXO adducts, the extent of mixing varying with the bending angle and with the vibrational frequencies. Nevertheless, DFT does a good job of reproducing the observed backbonding trends in model adducts having varying electron-withdrawing and -donating porphyrin substituents.

Table 4. Optimized (DFT, UBP86) Bond Lengths (Å), Bond Angles (deg), and Vibrational Stretching Frequencies (cm^{-1}) Obtained for the Five-Coordinate $Fe^{II}(OO)$ Porphine Adducts with Different β-Substituents

complex	Fe−OO	O−O	∠FeOO	Fe−N_p	ν(Fe−OO)	ν(O−O)
			5-c Fe(II)OO, UBP86 Functional (Open Shell Singlet)			
$FeP(NH_2)_8$	1.773	1.286	119.8	1.994/2.012	504.8	1230.5
$FeP(OH)_8$	1.770	1.285	119.7	1.993/2.008	506.8	1232.7
$FeP(NH_2)_4$	1.768	1.284	120.1	1.995/2.012	510.7	1234.1
$FeP(CH_3)_8$	1.766	1.283	120.3	1.994/2.010	512.9	1235.9
$FeP(CH_3)_4$	1.766	1.282	120.3	1.994/2.010	509.7	1239.3
$FePP(PropH)_2$	1.767	1.282	120.2	1.998/2.010	510.9	1240.2
FePH	1.766	1.281	120.3	1.994/2.010	509.1	1242.1
$FePF_4$	1.768	1.280	120.1	1.992/2.007	505.4	1246.8
$FePF_8$	1.770	1.279	119.9	1.990/2.005	504.0	1249.4
$FePCl_4$	1.769	1.279	120.1	1.996/2.011	503.6	1250.8
$FePCl_8$	1.771	1.277	120.0	1.998/2.013	505.9	1255.6
$FeP(NO_2)_4$	1.772	1.274	120.2	2.000/2.015	505.0	1263.8
$FeP(NO_2)_8$	1.777	1.270	120.1	1.994/2.011	501.3	1276.6

dx.doi.org/10.1021/ic400364x | Inorg. Chem. 2013, 52, 7478−7486

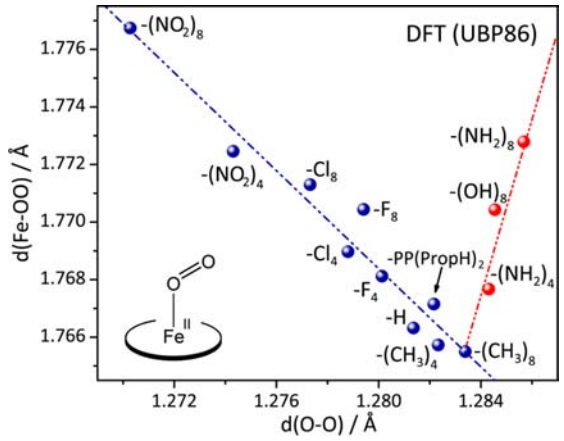

Figure 9. Fe−OO/O−O bond lengths correlation for the five-coordinate $Fe^{II}(OO)PX_8$ and $Fe^{II}(OO)PX_4$ models obtained from the spin-unrestricted DFT/UBP86 calculations.

However, accurate modeling requires the use of nonhybrid functionals that do not overemphasize the stability of high-spin states. Using BP86, we find that the ground state of $Co^{II}(NO)$ adducts is a closed shell singlet, consistent with the experimental structure. The computed Co−NO distance agrees with the experimental distance, whereas the computed distance for the open-shell singlet state is significantly longer.

The computed ground state for the isoelectronic $Fe^{II}(OO)$ adducts is the open-shell singlet, consistent with other studies.[37−41,63] In this case there is no experimental structure of a 5-coordinate $Fe^{II}(OO)$ adduct to provide guidance. However, DFT yields a ν(FeO)/ν(OO) backbonding slope that agrees well with experiment (leaving aside models with strongly electron-donating substituents), provided that the open-shell singlet ground state is used. Agreement is significantly poorer for the closed-shell singlet state. This connection to the vibrational frequency pattern provides support for the open-shell singlet indeed being the ground state.

A remarkable computational result is the reversal of the backbonding slope when electron-donating substituents are included in the correlation, when either frequencies (Figure 8) or bond distances (Figure 9) are plotted. For substituents more strongly donating than $-CH_3$, the Fe−O and O−O bonds become weaker together, contrary to backbonding expectations. This effect is not seen in the experimental data, which do not include adducts with electron-donating porphyrin substituents. (The O_2 adducts are unstable, quickly oxidizing in solution, and have only been examined via matrix isolation.)

How can one account for this reversal? As has often been pointed out, the open-shell singlet ground state implies a $Fe(III)O_2^-$ electronic structure, consistent with the Mossbauer parameters, and with the O−O stretching frequency itself, which is essentially that of superoxide (Supporting Information, Table S5). The main bonding interaction is σ donation from superoxide to Fe(III). This interaction is augmented by backbonding via overlap of the Fe d_{yz} and O_2 π_y^* orbital (y being the direction perpendicular to the FeOO plane). As electron donation from the substituents increases, backbonding is expected to increase, strengthening the Fe−O bond while weakening the O−O bond. This effect accounts for the inverse correlation. However, electron donating substituents also raise the energy of the porphyrin-Fe orbitals relative to those of the O_2 orbitals so that the d_{yz}-π_y^* overlap becomes smaller. This effect can be seen in the energy-level diagram in Supporting Information, Figure S9. At the same time, the increasing electron density on Fe diminishes σ donation from the superoxide, lengthening both the Fe−O and the O−O bonds. At some point, the σ effect becomes dominant, and the correlation becomes direct, rather than inverse. The computation indicates that this point corresponds to a model with $-(CH_3)_8$ substituents. For the three most electron-donating substituents, which define the direct branch of the correlation, the d_{yz}-π_y^* overlap is minimal, appearing only in the α-spin manifold (Supporting Information, Figure S9).

CONCLUSIONS

Five-coordinate FeXO porphyrin adducts (X = C, N, O) all show negative backbonding correlations with similar slopes between Fe−X and X−O mode frequencies, despite differing electronic and geometric structure, and despite the "ν(FeX)" mode being a mixture of Fe−X stretching and Fe−X−O bending coordinates when the FeXO geometry is bent. $Co^{II}(NO)$ adducts are likewise found to follow such a correlation.

DFT computations on model porphyrin adducts in which backbonding is modulated by the inductive effect of electron-donating or -withdrawing substituents, capture these correlations with good agreement of calculated and experimental slopes. For adducts with low-lying open-shell states (NO, O_2), nonhybrid functionals are required for good results. Using the nonhybrid BP86 functional, the ground state is found to be closed shell singlet for $Co^{II}(NO)$ adducts, but open shell singlet for the isoelectronic $Fe^{II}(OO)$ adducts. Agreement of calculated and experimental frequency correlations support these assignments.

For $Fe^{II}(OO)$ adducts, the ν(FeO)/ν(OO) correlation is predicted to be direct, rather than inverse, for substituents more electron donating than $-CH_3$. This reversal in slope is attributed to the dominance of superoxide-Fe(III) σ bonding when electron-donor substituents raise the porphyrin-Fe orbital energies sufficiently to make the backbonding π overlap ineffective.

ASSOCIATED CONTENT

Supporting Information

Complete references 46 and 47. Optimized bond lengths, MXO angle, and ν_{MX}/ν_{XO} vibrational stretching frequencies obtained with different DFT functionals and compared to selected experimental data for $Fe^{II}(NO)$ (Table S1), $Co^{II}(NO)$ (Table S2), and $Fe^{II}(OO)$ (Table S3) models. Experimental Fe^{II}−OO and O−O stretching frequencies of 5-coordinate $Fe^{II}(O_2)$ porphyrin adducts (Table S4). Theoretically obtained bond lengths and ν_{XO} for the O_2 and NO species together with the experimental values (Table S5). Fe^{II}−NO bonding description (Figure S1), RR and RR difference spectra ($^{14}NO - {}^{15}NO$) for $Co^{II}(NO)(TMeOPP)$ (Figure S2), $Co^{II}(NO)(TPPF_5)$ (Figure S3), $Co^{II}(NO)(TPP)$ (Figure S4), ν_{FeN}/ν_{NO} correlation plot computed for the 5-c $Fe^{II}(NO)$ complexes using DFT/UBLYP (Figure S5), Fe−NO/N−O bond length correlation for the 5-c $Fe^{II}(NO)$ adducts obtained with DFT/UBLYP and DFT/UBP86 (Figure S6), Co−NO/N−O bond length correlation for the 5-c $Co^{II}(NO)$ models obtained with DFT/BP86 (Figure S7), ν_{FeO}/ν_{OO} correlation and Fe−OO/O−O bond length correlation for the 5-c $Fe^{II}(O)_2$ models obtained from the DFT/BP86 calculations assuming a closed shell electronic

dx.doi.org/10.1021/ic400364x | Inorg. Chem. 2013, 52, 7478−7486

configuration (Table S8, Figure S8), and MO orbital energies and compositions for selected substituted $Fe^{II}(O_2)P$ adducts obtained from spin-unrestricted BP86 calculations (Figure S9). This material is available free of charge via the Internet at http://pubs.acs.org.

AUTHOR INFORMATION

Corresponding Author

*E-mail: spiro@chem.washington.edu.

Present Address

[†]Thermo Fisher Scientific Inc., 355 River Oaks Pkwy, San Jose, CA 95134.

Notes

The authors declare no competing financial interest.

ACKNOWLEDGMENTS

This work was supported financially by NIH Grant GM33567 to T.G.S.

REFERENCES

(1) Rodgers, K. R. *Curr. Opin. Chem. Biol.* **1999**, *3*, 158−167.
(2) Chan, M. K. *Curr. Opin. Chem. Biol.* **2001**, *5*, 216−222.
(3) Uchida, T.; Kitagawa, T. *Acc. Chem. Res.* **2005**, *38*, 662−670.
(4) Spiro, T. G. *Adv. Protein Chem.* **1985**, *37*, 111−159.
(5) Spiro, T. G.; Czernuszewicz, R. S.; Li, X.-Y. *Coord. Chem. Rev.* **1990**, *100*, 541−571.
(6) Ohta, T.; Kitagawa, T. *Inorg. Chem.* **2005**, *44*, 758−769.
(7) Spiro, T. G.; Ibrahim, M.; Wasbotten, I. H. In *The Smallest Biomolecules: Diatomics and Their Interactions with Heme Proteins*; Ghosh, A., Ed.; Elsevier: Amsterdam, The Netherlands, 2008; pp 95−123.
(8) Spiro, T. G.; Soldatova, A. V.; Balakrishnan, G. *Coord. Chem. Rev.* **2013**, *257*, 511−527.
(9) Xu, C.; Ibrahim, M.; Spiro, T. G. *Biochemistry* **2008**, *47*, 2379−2387.
(10) Spiro, T. G.; Soldatova, A. V. *J. Inorg. Biochem.* **2012**, *115*, 204−210.
(11) Spiro, T. G.; Wasbotten, I. H. *J. Inorg. Biochem.* **2005**, *99*, 34−44.
(12) Kozlowski, P. M.; Vogel, K. M.; Zgierski, M. Z.; Spiro, T. G. *J. Porphyrins Phthalocyanines* **2001**, *5*, 312−322.
(13) Ibrahim, M.; Xu, C.; Spiro, T. G. *J. Am. Chem. Soc.* **2006**, *128*, 16834−16845.
(14) Ghosh, A. *Acc. Chem. Res.* **2005**, *38*, 943−954.
(15) Soldatova, A. V.; Ibrahim, M.; Olson, J. S.; Czernuszewicz, R. S.; Spiro, T. G. *J. Am. Chem. Soc.* **2010**, *132*, 4614−4625.
(16) Linder, D. P.; Rodgers, K. R. *Inorg. Chem.* **2005**, *44*, 1367−1380.
(17) Linder, D. P.; Rodgers, K. R. *J. Biol. Inorg. Chem.* **2007**, *12*, 721−731.
(18) Walker, F. A. *J. Inorg. Biochem.* **2005**, *99*, 216−236.
(19) Almog, J.; Baldwin, J. E.; Huff, J. *J. Am. Chem. Soc.* **1975**, *97*, 227−228.
(20) Collman, J. P. *Acc. Chem. Res.* **1977**, *10*, 265−272.
(21) Momenteau, M.; Reed, C. A. *Chem. Rev.* **1994**, *94*, 659−698 , and references therein.
(22) Vogel, K. M.; Kozlowski, P. M.; Zgierski, M. Z.; Spiro, T. G. *J. Am. Chem. Soc.* **1999**, *121*, 9915−9921.
(23) Mizutani, Y.; Hashimoto, S.; Tatsuno, Y.; Kitagawa, T. *J. Am. Chem. Soc.* **1990**, *112*, 6809−6814.
(24) Bajdor, K.; Oshio, H.; Nakamoto, K. *J. Am. Chem. Soc.* **1984**, *106*, 7273−7274.
(25) Proniewicz, L. M.; Paeng, I. R.; Nakamoto, K. *J. Am. Chem. Soc.* **1991**, *113*, 3294−3303.
(26) Hu, S. Z.; Schneider, A. J.; Kincaid, J. R. *J. Am. Chem. Soc.* **1991**, *113*, 4815−4822.
(27) Bangcharoenpaurpong, O.; Rizos, A. K.; Champion, P. M.; Jollie, D.; Sligar, S. G. *J. Biol. Chem.* **1986**, *261*, 8089−8092.
(28) Sjodin, T.; Christian, J. F.; Macdonald, I. D. G.; Davydov, R.; Unno, M.; Sligar, S. C.; Hoffman, B. M.; Champion, P. M. *Biochemistry* **2001**, *40*, 6852−6859.
(29) Chottard, G.; Schappacher, M.; Ricard, L.; Weiss, R. *Inorg. Chem.* **1984**, *23*, 4557−4561.
(30) Das, T. K.; Couture, M.; Ouellet, Y.; Guertin, M.; Rousseau, D. L. *Proc. Natl. Acad. Sci. U.S.A.* **2001**, *98*, 479−484.
(31) Chartier, F. J. M.; Blais, S. P.; Couture, M. *J. Biol. Chem.* **2006**, *281*, 9953−9962.
(32) Lu, C.; Egawa, T.; Wainright, L. M.; Poole, R. K.; Yeh, S. R. *J. Biol. Chem.* **2007**, *282*, 13627−13636.
(33) Lu, C.; Egawa, T.; Batabyal, D.; Mukai, M.; Yeh, S. R. In *The Smallest Biomolecules: Diatomics and Their Interactions with Heme Proteins*; Ghosh, A., Ed.; Elsevier: Amsterdam, The Netherlands, 2008; pp 235−266.
(34) Mukai, M.; Savard, P.-Y.; Ouellet, H.; Guertin, M.; Yeh, S.-R. *Biochemistry* **2002**, *41*, 3897−3905.
(35) Manez, P. A.; Lu, C.; Boechi, L.; Marti, M. A.; Shepherd, M.; Wilson, J. L.; Poole, R. K.; Luque, F. J.; Yeh, S.-R.; Estrin, D. A. *Biochemistry* **2011**, *50*, 3946−3956.
(36) Sawai, H.; Yoshioka, S.; Uchida, T.; Hyodo, M.; Hayakawa, Y.; Ishimori, K.; Aono, S. *Biochim. Biophys. Acta* **2010**, *1804*, 166−172.
(37) Rovira, C.; Kunc, K.; Hutter, J.; Ballone, P.; Parrinello, M. *J. Phys. Chem. A* **1997**, *101*, 8914−8925.
(38) Sigfridsson, E.; Ryde, U. *J. Inorg. Biochem.* **2002**, *91*, 101−115.
(39) Jensen, K. P.; Ryde, U. *J. Biol. Chem.* **2004**, *279*, 14561−14569.
(40) Chen, H.; Ikeda-Saito, M.; Shaik, S. *J. Am. Chem. Soc.* **2008**, *130*, 14778−14790.
(41) Shaik, S.; Chen, H. *J. Biol. Inorg. Chem.* **2011**, *16*, 841−855.
(42) Sun, Y.; Hu, X. B.; Li, H. R.; Jalbout, A. F. *J. Phys. Chem. C* **2009**, *113*, 14316−14323.
(43) Liao, M.-S.; Huang, M.-J.; Watts, J. D. *J. Phys. Chem. A* **2010**, *114*, 9554−9569.
(44) Rovira, C.; Parrinello, M. *J. Quantum Chem.* **1998**, *70*, 387−394.
(45) Wilson, S. A.; Kroll, T.; Decreau, R. A.; Hocking, R. K.; Lundberg, M.; Hedman, B.; Hodgson, K. O.; Solomon, E. I. *J. Am. Chem. Soc.* **2013**, *135*, 1124−1136.
(46) Frisch, M. J.; et al. *Gaussian 09*, Revision B.01; Gaussian, Inc.: Wallingford, CT, 2010.
(47) Frisch, M. J.; et al. *Gaussian 03*, Revision E.01; Gaussian, Inc.: Wallingford, CT, 2004.
(48) Bauernschmitt, R.; Ahlrichs, R. *Chem. Phys. Lett.* **1996**, *256*, 454−464.
(49) Li, J.; Peng, Q.; Barabashnikov, A.; Pavlik, J. W.; Alp, E. E.; Sturhahn, W.; Zhao, J.; Schulz, C. E.; Sage, J. T.; Scheidt, W. R. *Chem.—Eur. J.* **2011**, *17*, 11178−11185.
(50) Goodrich, L. E.; Paulat, F.; Praneeth, V. K. K.; Lehnert, N. *Inorg. Chem.* **2010**, *49*, 6293−6316.
(51) Hu, S.; Kincaid, J. R. *J. Am. Chem. Soc.* **1991**, *113*, 9760−9766.
(52) Tomita, T.; Hirota, S.; Ogura, T.; Olson, J. A.; Kitagawa, T. *J. Phys. Chem. B* **1999**, *103*, 7044−7054.
(53) Dierks, E. A.; Hu, S.; Vogel, K. M.; Yu, A. E.; Spiro, T. G.; Burstyn, J. N. *J. Am. Chem. Soc.* **1997**, *119*, 7316−7323.
(54) Spiro, T. G. In *Iron Porphyrins, Part 2, Physical Bioinorganic Chemistry Series*; Lever, A. B. P., Gray, H. B., Eds.; Addison-Wesley: Reading, MA, 1983; pp 89−159.
(55) Vogel, K. M.; Kozlowski, P. M.; Zgierski, M. Z.; Spiro, T. G. *Inorg. Chim. Acta* **2000**, *297*, 11−17.
(56) Watanabe, T.; Ama, T.; Nakamoto, K. *J. Phys. Chem.* **1984**, *88*, 440−445.
(57) Rauhut, G.; Pulay, P. *J. Phys. Chem.* **1995**, *99*, 3093−3100.
(58) Ghosh, A. *J. Biol. Inorg. Chem.* **2006**, *11*, 712−724.
(59) Kuta, J.; Patchkovskii, S.; Zgierski, M. Z.; Kozlowski, P. M. *J. Comput. Chem.* **2006**, *27*, 1429−1437.
(60) Jaworska, M. *Chem. Phys.* **2007**, *332*, 203−210.
(61) Jaworska, M.; Lodowski, P. *Struct. Chem.* **2012**, *23*, 1333−1348.

(62) Selcuki, C.; van Eldik, R.; Clark, T. *Inorg. Chem.* **2004**, *43*, 2828−2833.
(63) Liu, Y.; Sun, H. *J. Comput. Chem.* **2011**, *32*, 1279−1285.
(64) Blomberg, L. M.; Blomberg, M. R. A.; Siegbahn, P. E. M. *J. Inorg. Biochem.* **2005**, *99*, 949−958.